MECHANICAL PROPERTIES OF MULTILAYERS OF CARBON NANOTUBE POLYSTYRENE NANOCOMPOSITES

A Thesis
Submitted to the Graduate Faculty
of the
North Dakota State University
of Agriculture and Applied Science

By

Eid Ali Almutairi

In Partial Fulfillment of the Requirements
for the Degree of
MASTER OF SCIENCE

Major Program:
Materials and Nanotechnology

April 2017

Fargo, North Dakota

North Dakota State University
Graduate School

Title

MECHANICAL PROPERTIES OF MULTILAYERS OF CARBON NANOTUBE POLYSTYRENE NANOCOMPOSITES

By

Eid Ali Almutairi

The Supervisory Committee certifies that this ***disquisition*** complies with North Dakota State University's regulations and meets the accepted standards for the degree of

MASTER OF SCIENCE

SUPERVISORY COMMITTEE:

Erik Hobbie
Chair

Yongki Choi

Wenfang Sun

Approved:

4/13/2017
Date

Erik Hobbie
Department Chair

ABSTRACT

We have studied the mechanical behavior of multi-layered composite films comprised of single-wall carbon nanotubes and polystyrene polymer, where we focused on three targeted layer thicknesses; 10 nm, 20 nm, and 40 nm. The approach we used is the Strain-Induced Elastic Buckling Instability for Mechanical Measurements (SIEBIFMM) technique, which allows us to measure the Young modulus of the films as a function of layer thickness and the number of layers by inducing a compressive stress in the films at different strains; 1 %, 2.5 %, 5 %, 7.5 %, and 10 %. Polystyrene was added in an effort to reduce the plasticity of the carbon nanotube films by filling the pores of the nanotube network. We found that the strongest synergistic effect in this regard occurred for the composite with a layer thickness near 20 nm, while the composite films have reached bulk behavior by the sixth layer.

ACKNOWLEDGEMENTS

I would like first to express my deep gratefulness for my advisor Professor Erik Hobbie. His valuable teaching and guidance enabled me to complete an important step in my academic career. His excellence in the field and his quick response to my questions allowed me to carry out the required research and improve my research skills. He is always a supportive and optimistic person. Also, I sincerely thank my colleagues who were more than friends to me; Meshal Alzaid, Matt Semler, Abu and Sam Brown, as well as all the other MNT program students. I will be forever grateful for your help and I wish you all the best in your life. I do not want to forget to thank my dear professors in my committee for their comments, Dr. Choi and Dr. Sun. Lastly, I am grateful to North Dakota State University for giving me this opportunity.

DEDICATION

To my lovely parents and my dear family

TABLE OF CONTENTS

LIST OF TABLES

LIST OF FIGURES

LIST OF APPENDIX FIGURES

1. INTRODUCTION

1.1. Flexible Electronics

Flexible electronics represent the future of the electronics industries. They have the potential to enable dramatic changes in our lives that conventional electronics cannot. Conventional electronics face major limitations relating to rigidity and cost. Most of our electronics, such as cell phones, televisions, and computer displays, are considered rigid materials, which suffer from cracks and failure when they are bent, twisted or faced with mechanical trauma. For instance, Indium Tin Oxide (ITO) is widely used in electronics for its high electrical conductivity, high optical transparency and ease of deposition [1]. However, despite ITO's strengths, ITO is brittle and has limited mechanical flexibility. As a result, alternatives to conventional electronics have to be explored. Ideally, flexible electronics can provide high mechanical flexibility, low weight, and high performance using low cost materials and processes.

Imagine if people could fold a TV, wear flexible devices on their hands, or incorporate them into their clothing. Flexible electronics have the potential to make these ideas a reality in the near future. Flexible electronics can also provide new possibilities in the biomedical field to raise the standards of care and health. For example, doctors could monitor a patients' physical status, such as heart rate or blood pressures, with more ease and comfort by designing flexible sensors that could be worn. These kinds of devices could be used in other areas as well, such as military and defense. For instance, soldiers would not need to carry heavy monitors for radar, maps or threat detection because these displays could be incorporated with their uniforms to make it easy and fast for them to access such data. Moreover, flexible electronics have great potential to be used in photovoltaic panels. People could literally roll-up their solar panels for

transport and use, rather than relying on rigid silicon panels, which are heavy and fragile [2]. To achieve this, it will be beneficial to use polymeric materials as a paradigm, since thin films made from such materials are flexible, durable, and easily processed.

1.2. Carbon Nanotubes

1.2.1. Structure

Carbon nanotubes (CNTs) have attracted much attention in recent decades because of their outstanding properties and myriad of potential applications. CNTs are long cylindrical covalently bonded carbon atoms that are formed by rolling a graphene sheet (a mono atomic sheet of carbon atoms) into tube. CNTs have a diameter of roughly 1 nm and an aspect ratio (length divided by diameter) of up to 1000. SWCNTs can be hollow open-ended cylinders or can be capped with hemifullerenes at one or both ends. Since the electronic configuration of a carbon atom is $1s^2\ 2s^2\ 2p^2$, and due to the small energy difference between 2*s* and 2*p* levels, a carbon atom can exist in different hybridization states, such as *sp*, sp^2 and sp^3. This variance in hybridization enables carbon atoms to arrange themselves in different allotropes, such as diamond (3D), graphite (2D), CNTs (1D) or fullerene (0D), as shown in Figure 1 [3].

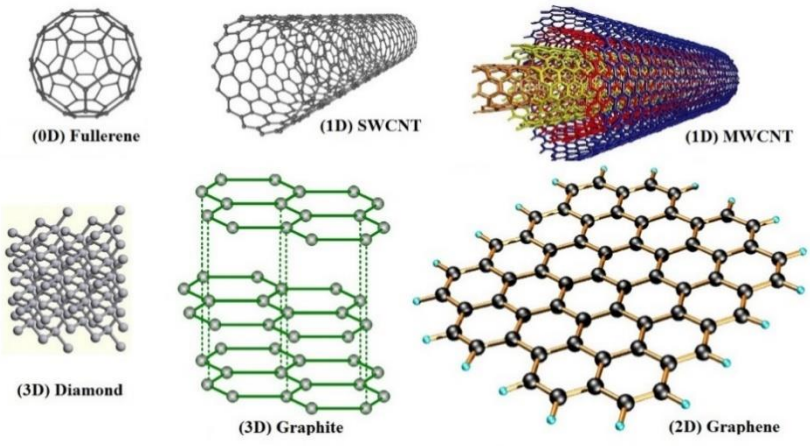

Figure 1. Carbon can form different allotropes due to variance in hybridization states [4].

CNTs were first reported by Iijima in 1991 [5]. There are two basic types of CNTs; multi-walled carbon nanotubes (MWCNTs) and single-walled carbon nanotubes (SWCNTs). Although the two materials are in some ways similar, a SWCNT is one cylinder while a MWCNT has more than one cylinder of CNTs around the core cylinder. For MWCNTs, the concentric cylinders have a radial spacing of 0.34 nm, which is close to the inter-plane spacing of graphite [6]. SWCNTs can be either metallic or semiconducting, which expands their range of applications. This variety is due to the wrapping of a graphene sheet, which is described by the chiral vector $\mathbf{c} = n\mathbf{a}_1 + m\mathbf{a}_2$, where the $\mathbf{a}_1$ and $\mathbf{a}_2$ are the basis vectors of graphene and the coefficients define the chiral index (n, m). As defined by the chiral vector, there are three general different ways for wrapping a graphene sheet. First, when the chiral indices are equal ($n = m$) and the chiral angle is 30°, the SWCNT is called "armchair". Second, when one of the chiral indices is zero (n, 0) or (0, m) and the chiral angle is 0°, the SWCNT is called "zig-zag". Third, when the chiral indices are not equal ($n \neq m$) and chiral angle is $0° < \theta < 30°$, the SWCNT is called "chiral". The chirality of the SWCNT determines many properties, but primarily the diameter and the band structure or electronic type [7].

1.2.2. Synthesis

CNTs are derived from a variety of synthesis methods and each method has advantages and disadvantages. First, there is the arc-discharge method, where a high current creates a temperature difference between two high-purity graphite electrodes, vaporizing one of the electrodes for deposition on the other. This method requires further purification of the CNTs to separate them from soot and other the residual carbon materials. A second method is laser ablation, where a pulsed laser is used to generate carbon atoms for deposition on a catalyst site or particle. Although the process is continuous, it is intrinsically low yield, which limits the

commercial potential. A third method is chemical vapor deposition (CVD), where a gaseous carbon source is deposited over a substrate in the presence of a metal catalyst. This method is not as expensive as the previous two methods and has the potential to be used widely in industry. In addition, it has other advantages, such as low power input and low temperature conditions. However, the produced CNTs are not high purity due to impurities from the metal substrate and the catalyst [8].

1.2.3. Properties

CNTs have a superb combination of mechanical, electrical, and thermal properties that make them excellent candidates to replace a large number of conventional materials currently used in the composites industry, or to make multifunctional composites. CNTs have a high electrical conductivity, where, theoretically, a metallic nanotube can carry a current density that is more than 1000 times greater than common metals, such as copper. Also, SWCNTs have a thermal conductivity almost 10 times higher than copper; 3500 $Wm^{-1} K^{-1}$ as compared to 385 $Wm^{-1} K^{-1}$ [9]. In addition, SWCNTs have a high tensile strength and Young modulus. This strength is attributed to the covalent sp^2 bonds between carbon atoms. The Young modulus can be on the order of 270 to 950 GPa, where the theoretical limit is up to 1 TPa [10], with a tensile strength of 11 to 63 GPa. A comparison of the tensile strength and Young modulus of individual CNTs with those of other materials in the bulk form is shown in Table 1 [11-17].

Table 1. Young modulus and tensile strength comparison between CNTs and other materials.

Material	Modulus (GPa)	Tensile Strength (MPa)
CNTs	650-1000	11,000-63,000
Copper	130	170
Steel	180	620
Polystyrene	3-3.5	40

1.3. Polystyrene

Polymers are broadly used in a variety of different industries, and polystyrene (PS) is one of the most common thermoplastics in our daily life. PS is a macromolecule with high molecular weight composed of many repeating units called monomers connected by chemical bonds. The PS monomer is styrene, or $C_6H_5CH=CH_2$. PS is an amorphous, glassy polymer that is generally rigid and brittle. It is naturally transparent, but it can be colored by adding pigments. It has a glass transition temperature of 100 ^oC, which makes it easy to process. The tensile strength of PS is 40 MPa, and the Young modulus is 3 to 3.5 GPa [17-18]. Also, PS is considered a hydrophobic material, so it is soluble in most organic solvents, such as toluene. The continuous bulk polymerization method is the most commonly used method for producing PS. In general, PS has different types with different properties due to the different processing techniques used to produce it. The most common type is expandable polystyrene (EPS) foam because it is extensively used in food containers, such as cups, lids and takeaway boxes. In addition, it is used in packaging and helmets. Most people mistakenly refer to EPS as Styrofoam, which is a brand name associated with the company that produced it, DOW Chemical. The second common type of PS is called extruded polystyrene (XPS), which is more rigid than EPS and is produced by extrusion as long sheets. XPS is mainly used in construction and buildings as a thermal insulator. There are other types of PS, such as high impact polystyrene (HIPS), which can absorb impact and is therefore used as a packing material for computers and other products [19].

According to the National Toxicology Program, the styrene monomer is suspected to be a carcinogenic material [20]. For that reason, much of the criticism related to PS comes from the fear of PS decomposing to its monomer and leaching into food products, which could happen

when PS is heated above its glass transition temperature. However, PS is thought to be safe because the percentage of styrene in PS is still under the minimum exposure limit [21].

1.4. Carbon Nanotubes Polystyrene Composites

The use of CNTs in composites creates new opportunities in the composites field, especially for polymer-CNT composites where the CNTs are used as reinforcement "filler" for the polymer. A relatively low loading of CNTs in a polymer matrix can increase its strength, Young modulus and thermal stability. CNTs can also transform an insulating polymer material into a conductor because of the high aspect ratio and low percolation threshold of CNTs. PS is a well-established thermoplastic and it has numerous applications, as mentioned above. The quality of the composite depends highly on the dispersion of individual CNTs in the polymer matrix, and this is a challenging process since CNTs are usually agglomerated in bundles because of strong attractive van der Waals interactions. Hence, there are different fabrication methods that can be used to prepare CNT/PS composites. First, solution mixing is a simple process involving mixing the CNTs and polymer in a suitable solvent and then removing the solvent by evaporation through drop casting or precipitation. As mentioned above, the dispersion of CNTs in the mixture is crucial for achieving optimal results, and this can be accomplished by using high-power ultra-sonication to disperse individual CNTs as a suspension. Second, melt mixing is a common polymer processing technique where the CNTs are mixed with the polymer prior to injection molding or extrusion. Melt mixing can produce composites in large scale and these techniques are widely used in the polymer industry. One study showed that adding just 0.2 wt. % of CNTs resulted in an approximately 8 MPa increase in the composite tensile strength [22]. However, the CNTs in these composites are not well bonded to the PS matrix because the interactions are mainly limited to weak van der Waals forces. Third, there is *in-situ*

polymerization, where the CNTs are mixed with styrene monomers and the CNT/PS composites are obtained by inducing polymerization in the presence of CNTs. One study suggested that when CNTs were coated with spherical PS nanoparticles, this led to a reduction in CNT agglomeration due to a suppression of van der Waals interactions between CNTs, thereby improving dispersion [23].

CNT/PS composites are currently very attractive materials for applications in the electronics, construction, aerospace and military fields. For instance, these composites can be used for strong and smart packaging or helmets with built in sensors. In military applications, the materials are of interest for electromagnetic shielding and absorption or frequency selective coatings. Moreover, these composites can be used as high-strength and low-density corrosion-resistant materials [24].

1.5. Research Approach

1.5.1. Fabrication Method

For SWCNT film fabrication, we used a vacuum filtration method to deposit the SWCNTs on a cellulose filter membrane. This method has several advantages besides its simplicity. First, it can generate highly uniform films through the use of surfactants and precursor solutions that have ideal SWCNT dispersion. Second, it is a precise method for producing SWCNT films with nanoscale thickness by control of the SWCNT concentration in the initial suspension. Third, it does not require expensive tools or volatile solvents, relying instead on water for the filtration process. As another advantage, it is possible to place a mask above the filter paper to achieve pattern formation for specific applications [25]. At the end of the process, acetone is used to dissolve the cellulous filter paper and release the film.

For composite fabrication, we used an approach different from the methods mentioned above. We made multilayers of SWCNT/PS nanosheets by alternating layers, beginning with a SWCNT layer and finishing with PS layer for up to six layers. We left intact an isolated portion of each layer of the composite for further characterization. Our approach is in some ways similar to layer-by-layer (LBL) assembly; however, we did not use any polyelectrolytes or coat the layers with opposite charges to generate electrostatic attraction between the layers, as is typically done in LBL [26]. The adhesion between layers in our research is mainly attributed to van der Waals forces. We used this method because a sheet-like composite geometry offers a simple structure that is easy to process and model, and it gives large contact area between the two components. Also, in our method, we can produce homogenous composites with a high weight and volume fraction of SWCNTs. In addition, our approach gives us precise control over the position on which to deposit the layers throughout the composite, which might be advantageous

for specific applications. As another advantage, nanoscale sheets provide a structural model for many hybrid materials, such as nanoscale heterojunctions comprised of semiconductors or metals for flexible electronics applications.

1.5.2. Characterization Technique

Conventional testing methods have long been used to determine the mechanical properties of materials in bulk form. However, it is known that the mechanical properties of thin films may be different from those of the bulk material, where this difference is due to the large surface to volume ratio typically encountered at the nanoscale. Here, we used a strain-induced elastic buckling instability for mechanical measurements (SIEBIMM) technique to measure the Young modulus of our SWCNT/PS composite films. Buckling or wrinkling is common in our daily life, such as for aging human skin or the dried skin of fruit, for example. In response to an applied compressive stress, thin films produce wrinkles with a varied periodicity that is directly related to the mechanical properties of the film [27]. These wrinkles have different length scales according to the mechanical properties of the materials and the nature of the strain that induces the wrinkles, which can be from thermal expansion, mechanical stretching, or solvent swelling. A schematic of the strain induced buckling of a thin polymer film on an elastic polydimethylsiloxane (PDMS) substrate is shown in Figure 2.

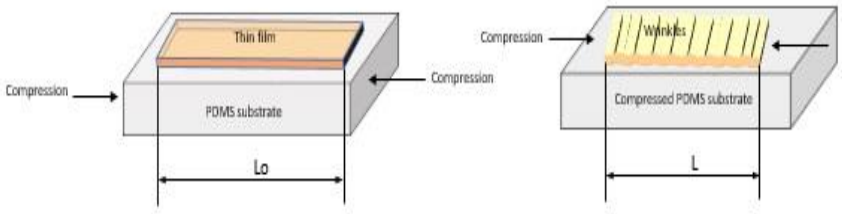

Figure 2. Schematic of the compression induced buckling of a thin polymer film on a PDMS substrate.

We chose the SIEBIMM technique to determine the mechanical properties of our thin-film materials because it is a simple and inexpensive method, compared to nanoindentation, for example. Also, it has another advantage over nanoindentation because it avoids uncertainties associated with indentation depth and the proximity of the substrate, which can lead to errors in the measured elastic modulus. At least in principle, the method is very simple. The mechanical properties can be obtained by applying a strain to a thin film adhered to a soft elastic substrate, which in our case is PDMS. By characterizing the wavelength and the amplitude of the resulting wrinkles, we can extract information about the modulus of the film. Since the earlier work of Whitesides and co-workers at Harvard University, many research studies have been conducted to study the buckling mechanism [28]. A knowledge of the wrinkling wavelength, film thickness, the Poisson ratios and the Young modulus of the substrate are enough to then get the Young modulus of the film, without the need to construct stress-strain curves, through the following equation:

$$\bar{E}_f = 3\,\bar{E}_s \left(\frac{\lambda}{2\pi h}\right)^3 \qquad (1)$$

where λ is the wavelength of the harmonic wrinkles, h is the film thickness, and $\overline{E}_{\mathrm{i}} = \frac{E_i}{(1-\nu_i^2)}$ is the plane-strain modulus, where i can denote the substrate ($i = s$) or the film ($i = f$), and ν is the Poison ratio [29]. With sufficient characterization of the quantities on the right-hand-side of Eq. (1), accurate results can be obtained using this technique. Rogers and coworkers have measured the Young modulus of oriented individual SWCNTs on a PDMS substrate using this technique. For tubes with diameters of 1-3 nm, they got a SWCNT Young modulus of 1.3 TPa ± 0.2 TPa, which is in good agreement with previous atomic-force microscopy (AFM) measurements [30].

We believe that this technique has invaluable implications for the characterization of nanoscale coatings in applications such as sensors and flexible electronics.

1.6. Objective

Several prospective materials have been proposed to overcome the rigidity obstacle of conventional electronics. In particular, novel materials, such as CNTs and graphene, are promising candidates due to their superb mechanical, electronic, thermal and optical properties. Despite their unique properties, which make them ideal for such applications, more research is needed to study film rigidity and durability for these novel materials. CNT films are considered semi-porous structures with strong van der Waals attractions that can be associated with large aspect ratios. CNT interactions in the film are predominantly van der Waals attraction and excluded-volume repulsion, while the limited sliding friction inherent to CNTs allows them to align in bundles in a direction perpendicular to the applied stress, leading to a phenomenon called strain softening. Strain softening reduces the rigidity of CNT films significantly when they are compressed and can impact the electrical conductivity as well [31]. Because of the poor translation of individual CNT properties to their macroscopic forms, most of the current applications involving CNTs only use CNTs as a reinforcement material for polymers matrices or other materials in the form of alloys, composites or hybrids ("blends"). For that, understanding the mechanical characteristics of CNTs in thin-film form would be very useful for emerging fields such as flexible electronics.

While many studies have focused on reinforcing polymers by mixing in CNTs, our study focused on a mutual reinforcing mechanism, where not only the excellent properties of CNTs will reinforce the polymer, but the polymer will also reduce strain softening of the CNTs by filling the pores of the CNT network [32]. In this research, we used the buckling approach to

study the mechanical behavior of six-layer nanosheet composites of SWCNT and PS on a soft substrate by measuring the Young modulus as a function of the layer thickness and the number of layers for different targeted layer thicknesses of 10, 20, and 40 nm. Also, we wanted to know the optimal layer thickness that would result in the optimum behavior. We can then relate this thickness to the width of the diffuse CNT-polymer interface. TEM images of this interface are shown in Figure 3.

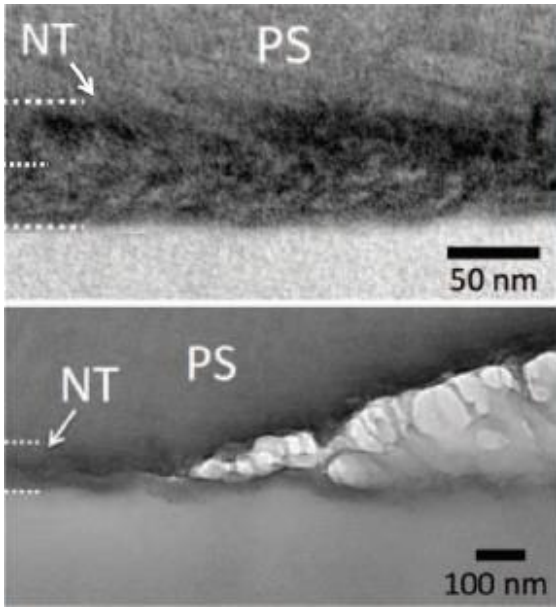

Figure 3. Cross-sectional TEM image of the SWCNT-PS interface for a 60 nm thick SWCNT film. The bottom image shows how SWCNTs are displaced when PS is peeled off the SWCNT layer [33].

2. EXPERIMENTAL PROCEDURE

2.1. Sample Preparation

2.1.1. Carbon Nanotubes

CoMoCat SG65i SWCNTs with a mean diameter near 0.75 nm and an aspect ratio of ~ 900 were used. A roughly 1 mg SWCNT/ml aqueous solution in 2 % mass fraction sodium deoxycholate (DOC) surfactant were dispersed using tip sonication (Thomas Scientific, 0.64 cm tip) for 1 hour in ice water at 1 W/mL power. After sonication, we used centrifugation for 2 hours at an acceleration of 21000*g* to remove large SWCNT bundles and impurities. In order to get the length distribution, we cleaned a small piece of wafer silicon with DI water and ethanol and then soaked it for 24 hours in a refrigerated solution consisting of 30 μl of stock aqueous SWCNT solution mixed with 150 μl DI water. Then, the silicon was soaked in ethanol for 2 hours. The length (*L*) distribution was measured using AFM (Agilent Technologies Model 5500) operated in tapping mode, where the mean length was of 670 nm. Films of nanoscale thickness were produced using vacuum filtration, as shown in Figure 4.

Figure 4. Vacuum filtration was used to produce SWCNT films with nanoscale thickness.

First, we soaked a cellulose filter paper (0.05 um, VMWP) in aqueous solution with 5 % ethanol for 2 hours in a petri dish. Every part of the vacuum filtration system was then washed with deionized water. Then, we put the glass filter on the flask and adjusted the level using a bubble level because unbalanced orientation will lead to concentration gradient in the film. Then, we placed the filter paper over the glass filter. After we assembled the components of the filtration system, we poured 200 ml of deionized water inside the beaker and let it settle for 2 minutes to remove any bubbles. We prepared SWCNT films of different thickness by varying the SWCNT concentration in the initial suspension. For example, to get a 10 nm film thickness, a volume of 3.6 µl of SWCNT solution was taken by a pipette and mixed with 496.4 µl of deionized water in a clean vial to yield a total volume of 500 µl. Using the pipette, we slowly deposited the 500 µl solution on the center of the cellulose filter paper, which helps to uniformly disperse the SWCNTs over the filter to produce a uniform surface coating. We let the solution equilibrate for 15 min before applying a vacuum. After applying vacuum for 1-2 hour, all the solution was pulled through the filter and a uniform film of SWCNT was obtained. We waited for 20 minutes until the surface was dry, and then we removed the SWCNT filter paper assembly using tweezers. An example of the film obtained is shown in Figure 5.

Figure 5. A thin SWCNT film on cellulose filter paper.

To get freestanding films, we cut three rectangular sections of different length (long, medium and short) using a scissors. The longest film was used for the first layer, the medium length was used for the third layer and the shortest length was used for the fifth layer. Then, we transferred films of comparable length to a separate vial of acetone for 1 hour to dissolve the filter paper backing. After 1 hour, we transferred them again to another acetone vial for another 1 hour. The purpose of the first acetone vial was to dissolve the majority of the filter paper while the purpose of the second vial was to make sure all the filter paper was dissolved. Next, we transferred the freestanding films to an ethanol vial to remove any residual surfactants still in the SWCNT film. The transferring method is unique and was developed in our laboratory by collecting the SWCNT film with a pipette. An example of freestanding SWCNT films in a vial and pictures depicting the transfer method are shown in Figure 6.

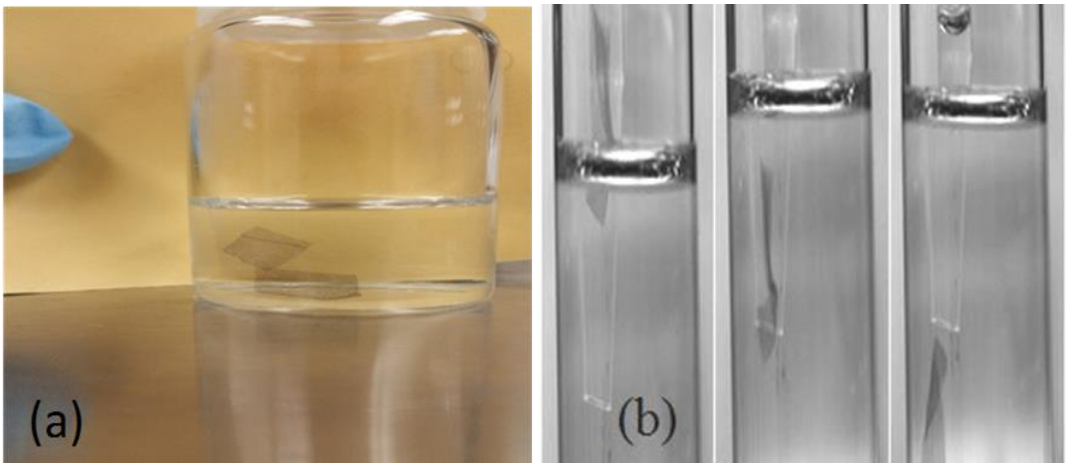

Figure 6. a) Freestanding SWCNT films in a vial. b) Transferring SWCNT films using a pipette.

2.1.2. Polystyrene

For the thin PS films, a measured mass of a PS standard (M_W = 213600, M_N = 211400, SIGMA-ALDRICH) was placed in a clean vial. The PS was dissolved with toluene at a concentration of

$$\phi = \frac{m_{ps}}{m_{ps}+m_t} \quad (2)$$

where m_{ps} is the mass of the PS and m_t is the mass of the toluene. A concentration of 1.44 % gives a PS film of 40 nm thickness, 0.72 % gives 20 nm thickness, and 0.36 % gives 10 nm thickness. After we mixed the components and the PS had dissolved, we stirred the solution for 15 minutes to ensure that the PS was uniformly distributed. Then, we placed a thin mica slide over a glass slide and put them inside a spin coater set at 3000 RPM (Figure 7).

Figure 7. Spin coater was used to produce PS films with nanoscale thickness.

With the slide spinning, two drops of the PS solution were deposited using a glass pipette and spun for 30 seconds. Next, we slowly immersed the mica slide into a glass beaker of deionized water to separate the PS film from the mica. This occurs readily because the mica is hydrophilic while in contrast the PS is hydrophobic. Floating PS films can be obtained through this method that possess nanoscale thicknesses, and which can later be transferred to the PDMS by "scooping" up the floating PS film with a mica slide. We made several sets of films at three targeted thicknesses; 10, 20, and 40 nm.

2.1.3. PDMS

Polydimethylsiloxane PDMS (Sylgard 184, Sigma-Aldrich) substrates were used for the strain experiments. The substrates were prepared by mixing a 10:1 ratio of PDMS monomer to cross-linker in a polymer beaker. The ratio was chosen to get a modulus E_s of close to 2 MPa, and the total volume of monomer used was chosen to achieve a thickness of 2 mm in a 10 cm x 20 cm glass mold. After pulling vacuum to get the air out of the liquid resin, the PDMS was heated for 2 hours at 90 ^{o}C. The plate was then removed, cooled, and cut into 1" x 3" slabs. To determine the Young modulus of the PDMS substrates, we used an Instron 5545 Tensile Tester with a 100 N load cell. The instrument measured the strain in the PDMS slabs over a series of applied loads. The Young modulus was calculated from the slope of the linear (small strain) portion of the stress *vs* strain curve. This was done for every PDMS substrate after each wrinkling experiment, with all values in the range $1.8 < E_s < 2.5$ MPa.

2.2. SWCNT/PS Composites

2.2.1. On PDMS

We cleaned a rectangular PDMS slide with dimensions (26.12 x 82.62 x 1.5) mm using distilled water and soap. We mounted the PDMS on the strain stage at each end with screw clamps. The strain stage is shown in Figure 8.

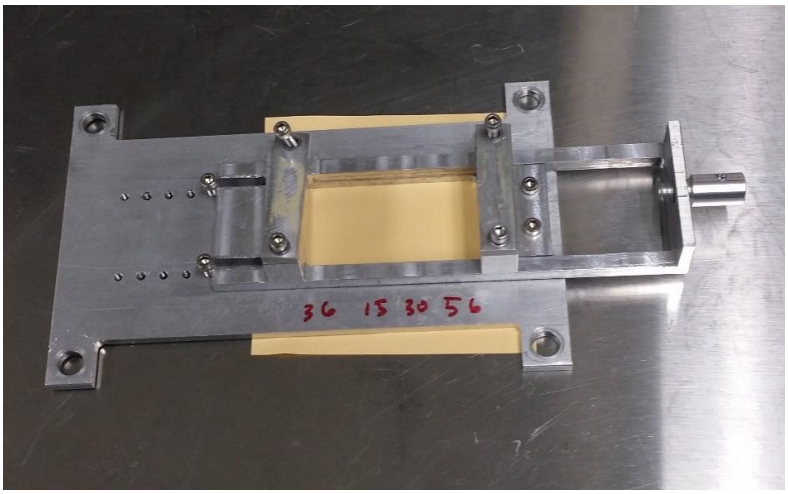

Figure 8. Strain stage was used to induce different strains in the PDMS composites.

We applied 15 % pre-strain to the PDMS. Then, we deposited the first SWCNT layer (the longest one) on the PDMS from ethanol using a pipette. By blowing air from the pipette to generate thrust, we moved the film to the target site on the PDMS and fully unfurled it before the ethanol evaporated. After the SWCNT film had dried and adhered to the PDMS, we collected the longest floating PS film (of the same target thickness) on a clean mica slide and gently pressed it against the first SWCNT layer and the PDMS, each time leaving an exposed area for further characterization. We repeated the steps for successively shorter lengths of both the SWCNT and PS until we made a composite of six layers; three SWCNT layers and three PS layers. We define n as the layer number, so that n = 1, 3, 5 are SWCNT films, and n = 2, 4, 6 are PS films, as depicted in the schematic composite structure of Figure 9.

Figure 9. Schematic structure of a six-layer SWCNT/PS nanosheet composite.

2.2.2. On Silicon

We made the same composite films on a silicon wafer to facilitate measuring the thickness of the layers using AFM. We cleaned small silicon rectangles with distilled water and soap. We placed the first SWCNT layer on the silicon using a pipette in the same manner as we did with the PDMS supported composite films. Then, we placed the silicon under vacuum for 30 minutes to make sure that the SWCNT film was well adhered to the silicon. After the SWCNT film dried, we held the silicon substrate with tweezers and immersed it in a beaker of distilled water containing the floating PS films. We carefully placed the longest floating PS film over the first SWCNT layer by gently scooping the floating PS film onto the silicon, again leaving an exposed area of the first SWCNT layer for later AFM measurements. We repeated the steps for the various lengths of both SWCNT and PS up to a composite of six layers; three SWCNT layers and three PS layers, identical to the PDMS composite films. To measure the thickness, we used a Veeco DI-3100 atomic force microscope (AFM) operated in tapping mode with an NT-MDT FMG01 probe (tip radius of 10 nm).

2.3. Induced Strain

For each targeted layer thickness, we made the two composite films – on PDMS and silicon – which were placed together in a vacuum-oven to anneal the films. We heated the samples to 100 ^{o}C, in the vicinity of the glass temperature of PS, to promote the infiltration of polymer into the SWCNT network. After the samples had cooled, we initiated the PDMS experiments and stored the silicon sample for later analysis. The strain in the PDMS substrate was released using a micrometer adjustment so as to introduce a 1 % compressive strain in the film. A set of reflection optical micrographs at 50x magnification were collected for each layer of each composite using an Olympus TH4-100 optical microscope to characterize the wrinkling topography of each compressed layer. The process was then repeated at 2.5 %, 5 %, 7.5 % and 10 % compressive strain. The SWCNT and PS films of targeted 10 nm thicknesses were more fragile than the other films and were very challenging to handle and process.

3. RESULTS AND DISCUSSIONS

There were small wrinkles induced in the thermal annealing step but these were isotropic and easy to be distinguished from the wrinkles, ridges and folds induced by the strain stage, which were oriented perpendicular to the direction of applied strain. We used ImageJ to count the wrinkling wavelength of each image for each layer of the three different thicknesses. The SWCNT/PS images of the six layers of the composites had a disordered wrinkling pattern that was different from PS films. For measuring the wavelength, we looked for uniform periodic patterns, which we refer to as the fundamental wrinkling mode. Figure 10 shows typical wrinkling patterns for some pure PS films, pure SWCNT films (n = 1) and SWCNT/PS composite films.

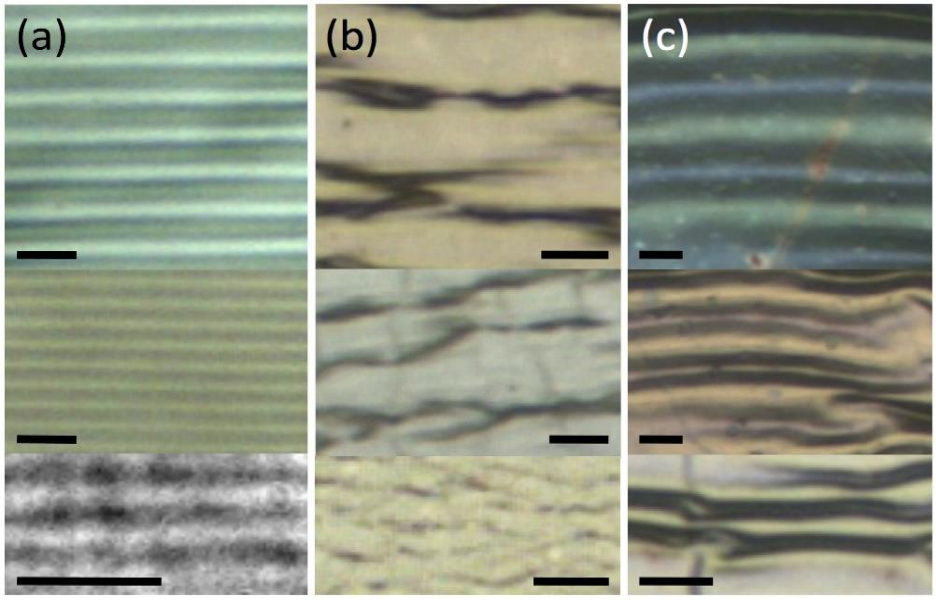

Figure 10. (a) Reflection optical micrographs of compressed polymer films on PDMS; h_0 = 75 nm (top), 37 nm (middle) and 12 nm (bottom). (b) Similar images for pure SWCNT films where h_0 is approximately 40 nm (top), 20 nm (middle) and 15 nm (bottom). (c) Optical images of wrinkling in a triple bilayer (n = 6, $h \approx$ 120 nm, top), a double bilayer (n = 4, $h \approx$ 78 nm, middle) and a bilayer (n = 2, $h \approx$ 41 nm, bottom) on PDMS. The scale bar in each image is 5 μm and the strain is 5 % compression in the vertical direction [34].

The disordered wrinkling pattern is due the presence of localization and bifurcation, which mitigates the overall stress of the film. Bifurcation can arise from inhomogeneity in the films or defects. When a defect is present, it disrupts the direction of the periodic pattern and localizes the deformation either around it (if the defect represents a weal point in the film, *e.g.* a drop in thickness) or away from it (if the inhomogeneity represents a strong point in the film, *e.g.* a jump in thickness). Also, these localizations have wrinkles with higher amplitude than their neighboring wrinkles because they combine together producing ridges or folds. These merged wrinkles always appear as black ridges in the reflection image, where the fundamental wrinkles of wavelength λ_0 are faint. Because the SWCNT films are more inhomogeneous, we do not see as uniform a pattern of wrinkles as we see for PS films, and in some cases we have to account for double or even quadruple the wavelength, since these ridges or folds contain more than one fundamental period (Figure 11).

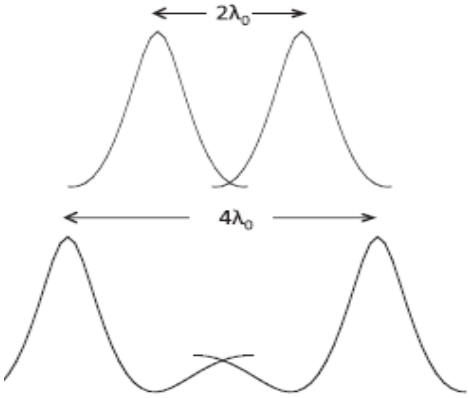

Figure 11. Schematic of bifurcation in an inhomogeneous film [35].

It was clear that the wavelength or characteristic length scale of the wrinkling deformation is decreasing with increasing strain. In contrast, the wavelength is increasing with increasing layers due to increasing thickness. We were able to locate the fundamental wrinkling pattern and the corresponding wavelength (λ_0) for all but the smallest strains of the thinnest

layers, such as the first layer (n = 1) of the 10 nm and 20 nm layer composites. For these, we had to account for doubling to get physical values of the modulus. The thickness values of each layer of the three composites were measured by using AFM, as shown in Table 2.

Table 2. The thickness of each layer as determined by AFM.

h (nm)	n = 1	n = 2	n = 3	n = 4	n = 5	n = 6
10	14.6 ± 0.6	10 ± 0.5	11 ± 0.6	10.4 ± 0.5	14.4 ± 0.6	11 ± 0.5
20	20.5 ± 1.0	20.6 ± 0.8	18.4 ± 1.0	18.7 ± 0.8	19.8 ± 1.0	21.5 ± 0.8
40	40.3 ± 2.0	42.3 ± 1.0	40.0 ± 2.0	41.6 ± 1.0	41.3 ± 2.0	40.8 ± 1.0

Using the measured wrinkling length scale and the measured thickness, we applied the strain-induced elastic buckling instability equation (1) to measure the Young modulus for each layer of the three sets of composite films. We assumed a Poisson ratio of v = 0.48 for PDMS, v = 0.33 for the SWCNT, and v = 0.33 for the polymer based on previous work [36-39]. As noted above, the modulus of the PDMS substrate was measured using an Instron 5545 Tensile Tester and fell within the range ($1.8 \leq E_s \leq 2.5$) MPa. Because we have a large number of Young modulus values as a function of layer thickness (h_0), layer number (n), and strain, Figure 12 presents the values of Young modulus of each layer as different colored markers representing a range of values.

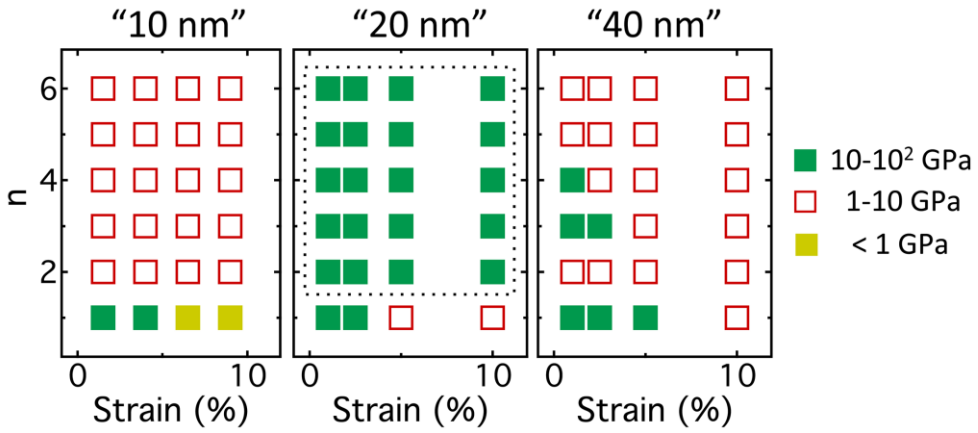

Figure 12. Strain dependent modulus in the plane of strain and the number of layers for each targeted layer thickness. Dark closed markers (green) denote 10-10^2 GPa, open (red) markers are 1-10 GPa, and light closed markers (yellow) are < 1 GPa. Regions within the dashed boundaries correspond to the optimum response [40].

From the graph, we can see that the higher Young modulus values were obtained at 20 nm layer thickness. In a separate experiment, we measured the modulus of pure PS polymer on PDMS, with the same targeted thicknesses as the composites films, to compare the Young modulus of the pure polymer to the composites. The results are plotted in Figure 13.

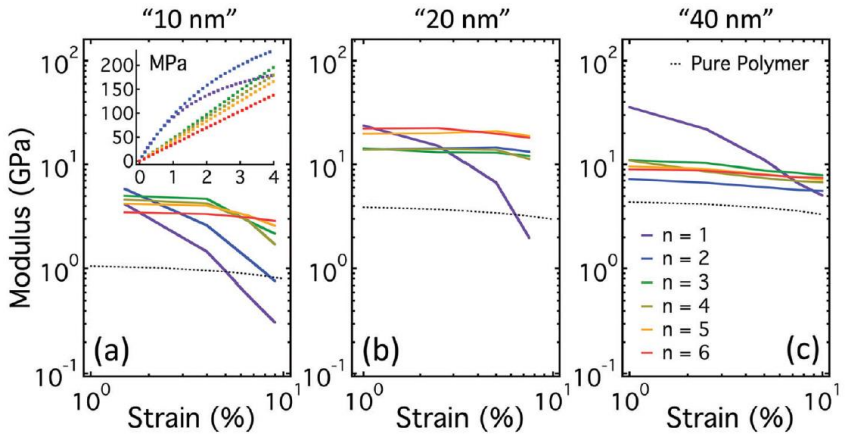

Figure 13. Modulus of the lamellar nanosheets as a function of strain for (a) the '10 nm', (b) '20 nm', and (c) '40 nm' datasets. The dashed line in each panel is the nonlinear elastic response based on the measured modulus of the pure polymer near the labeled thickness. The inset to (a) shows the computed stress-strain curve corresponding to the yield strain and modulus extracted from the response [40].

The data demonstrate that strain softening is significant in all n = 1 films, where the Young modulus of first SWCNT layer dropped steeply with increasing strain. Also, there is a degree of strain softening evident in the second layer (n = 2) of the thinnest layer thickness, h_0 = 10 nm. On the other hand, we can see how the polymer reduced the strain softening in the layers following the first layer, especially in the 20 nm composite. This is can be explained by the PS film filling the pores of the SWCNT network, which mitigates van der Waals interactions between the nanotubes through an excluded volume effect and reduces the plasticity of the films. Comparing the values with the pure polymer, we see that the SWCNT enhanced the stiffness of the composite for all thicknesses. In addition, there is a drop in the PS modulus below 40 nm, which is in agreement with previous studies [38,41].

We modeled the layers that have significant strain softening using the following equation to get zero strain modulus:

$$E(\varepsilon) = E_0 \left(1 + \frac{\varepsilon}{\varepsilon_0}\right)^{-\delta} \quad (3)$$

where δ = 3 is a critical exponent, ε is the applied strain, ε_0 is the yield strain, and E_0 is the modulus in the zero-strain limit [42]. As might be anticipated, the modulus for n = 6 is intermediate to the moduli of the pure materials. To quantify this, we note that the lamellar geometry is ideal for a simple rule of mixtures, which has two limits that represent upper and lower bounds. The upper bound [$E_{||} = \phi E_{CNT} + (1-\phi)E_{Poly}$] models uniform strain (so-called "ideal" behavior), while the lower bound [$1/E_{\perp} = \phi/E_{CNT} + (1-\phi)/E_{Poly}$] models uniform stress (nonideal behavior) [43]. Because the layers of a nanosheet all have close to a common thickness h_0, the volume fraction is close to 0.5. We use the measured SWCNT (purple curve, Figure 14) and polymer (gray curve, Figure 14) modulus for E_{CNT} and E_{Poly}, respectively. The resulting upper and lower bounds are indicated in Figure 14 (black dashed).

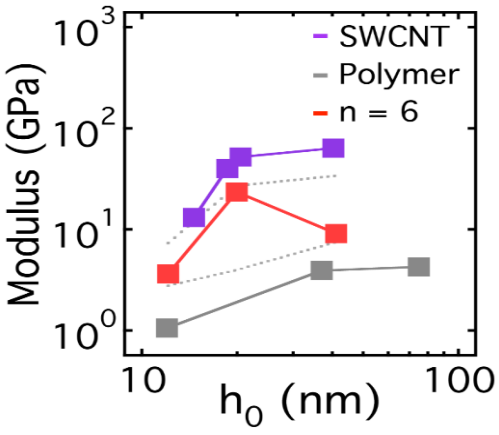

Figure 14. Extrapolated zero-strain modulus as a function of layer thickness for the pure SWCNT (*n* = 1), pure polymer, and the triple bilayer composite (*n* = 6). The dashed lines are the upper and lower bounds detailed in the text. Error bars are the size of the data markers [44].

The results demonstrate that the *n* = 6 behavior is constrained between the upper and lower bound, which means by the sixth layer, we have reached essentially bulk-like behavior. Also, we can see that the zero-strain modulus of the pure SWCNT (*n* = 1) is increasing with increasing thickness, consistent with previous studies [37,42]. At layer thicknesses of 20 nm and 10 nm, the performance is closer to ideal behavior as compared to 40 nm layer thickness.

4. CONCLUSION

In conclusion, we have used a strain induced wrinkling approach to study the mechanical behavior of multi-layered composite films comprised of alternating nanoscale SWCNT and PS layers as a function of layer thickness and number of layers. Our results suggest that the films exhibit the greatest mechanical synergy near the layer of thickness 20 nm, based on the higher Young modulus values, ideal behavior and a suppression of SWCNT film plasticity. We attribute this to the proximity of this layer thickness to a width of a SWCNT/PS interface. Although the 10 nm layer thickness is even smaller, we suspect that the response measured for this data set is influenced by thickness inhomogeneities in the SWCNT layer, which impact film rigidity because of the close proximity to the percolation threshold. For all layer thicknesses (10, 20, and 40 nm), the behavior of the composite films has essentially realized close to bulk behavior by the sixth layer. It is very encouraging to get enhanced mechanical properties of composites that have been assembled from incompatible components, such as SWCNTS and PS, without the need for chemical modification, such as conventional crosslinking. Based on our results, we have demonstrated the optimum layer thickness for enhanced mechanical behavior in multilayer SWCNT/PS composite films, and we hope that these results will have useful implications for controlling the rigidity and the durability of a variety of lamellar nanosheets, including hybrid heterojunctions and flexible electronic devices.

In terms of the outlook for future research, more research is needed to further clarify the rigidity of CNT composites films and better understand their mechanical behavior. Extending the width of the interface is necessary to further enhance the performance, especially in approaches like ours that do not rely on chemical crosslinking between the composite components. Another important aspect of this idea is the use of additional fillers beyond polymers such quantum dots,

PEDOT:PSS, or metallic nanoparticles that have better electrical properties, which offer the promise of enhanced mechanical properties coupled with enhanced electronic properties.

REFERENCES

[1] H. Kim, C. M. Gilmore, A. Piqué, J. S. Horwitz, H. Mattoussi, H. Murata, Z. H. Kafafi, and D. B. Chrisey, "Electrical, optical, and structural properties of indium–tin–oxide thin films for organic light-emitting devices," *Journal of Applied Physics*, vol. 86, no. 11, pp. 6451–6461, 1999.

[2] "Flexible Electronics," *Electronic Materials: Science & Technology,* 2009.

[3] W. Khan, R. Sharma, and P. Saini, "Carbon Nanotube-Based Polymer Composites: Synthesis, Properties and Applications," *Carbon Nanotubes - Current Progress of their Polymer Composites,* 2016.

[4] N. F. Atta, A. Galal, and E. H. El-Ads, "Graphene — A Platform for Sensor and Biosensor Applications," Biosensors - Micro and Nanoscale Applications, 2015.

[5] S. Iijima, "Helical microtubules of graphitic carbon," *Nature,* vol. 354, no. 6348, pp. 56–58, Jul. 1991.

[6] M. Moniruzzaman and K. I. Winey, "Polymer Nanocomposites Containing Carbon Nanotubes," *Macromolecules*, vol. 39, no. 16, pp. 5194–5205, 2006.

[7] W. Khan, R. Sharma, and P. Saini, "Carbon Nanotube-Based Polymer Composites: Synthesis, Properties and Applications," *Carbon Nanotubes - Current Progress of their Polymer Composites,* 2016.

[8] K. Awasthi, A. Srivastava, and O. N. Srivastava, "Synthesis of Carbon Nanotubes," *Journal of Nanoscience and Nanotechnology*, vol. 5, no. 10, pp. 1616–1636, Jan. 2005.

[9] S. Hong and S. Myung, "Nanotube Electronics: A flexible approach to mobility," *Nature Nanotechnology*, vol. 2, no. 4, pp. 207–208, 2007.

[10] M. Yu, “Strength and Breaking Mechanism of Multiwalled Carbon Nanotubes Under Tensile Load,” *Science*, vol. 287, no. 5453, pp. 637–640, 2000.

[11] R. H. Baughman, “Carbon Nanotubes--the Route Toward Applications,” *Science*, vol. 297, no. 5582, pp. 787–792, Feb. 2002.

[12] R. S. Ruoff, D. Qian, and W. K. Liu, “Mechanical properties of carbon nanotubes: theoretical predictions and experimental measurements,” *Comptes Rendus Physique*, vol. 4, no. 9, pp. 993–1008, 2003.

[13] H. M. Ledbetter and E. R. Naimon, “Elastic Properties of Metals and Alloys. II. Copper,” *Journal of Physical and Chemical Reference Data*, vol. 3, no. 4, pp. 897–935, 1974.

[14] W. Jenkins, T. Digges, and C. Johnson, “Tensile properties of copper, nickel, and 70-percent-copper-30-percent-nickel and 30-percent-copper-70-percent-nickel alloys at high temperatures,” Journal of Research of the National Bureau of Standards, vol. 58, no. 4, p. 201, 1957.

[15] S. W. Banovic, C. N. Mccowan, and W. E. Luecke, “Physical properties of structural steels,” 2005.

[16] K. Miyake, N. Satomi, and S. Sasaki, “Elastic modulus of polystyrene film from near surface to bulk measured by nanoindentation using atomic force microscopy,” *Applied Physics Letters*, vol. 89, no. 3, p. 031925, 2006.

[17] “Tensile Property Testing of Plastics,” *Tensile Property Testing of Plastics*. [Online]. Available: http://www.matweb.com/reference/tensilestrength.aspx. [Accessed: 07-Apr-2017].

[18] W. E. Wallace, J. H. V. Zanten, and W. L. Wu, “Influence of an impenetrable interface on a polymer glass-transition temperature,” *Physical Review E*, vol. 52, no. 4, Jan. 1995.

[19] E. Jakab, M. Uddin, T. Bhaskar, and Y. Sakata, “Thermal decomposition of flame-retarded high-impact polystyrene,” Journal of Analytical and Applied Pyrolysis, vol. 68-69, pp. 83–99, 2003.

[20] “Review of the Styrene Assessment in the National Toxicology Program 12th Report on Carcinogens,” 2014.

[21] J. P. H. Linssen, J. C. E. Reitsma, and J. P. Roozen, “Effect of sampling method on the level of styrene monomer migrated from polystyrene packaging material,” *Packaging Technology and Science*, vol. 4, no. 3, pp. 171–175, 1991.

[22] M. Kaseem, K. Hamad, and Y. G. Ko, “Fabrication and materials properties of polystyrene/carbon nanotube (PS/CNT) composites: A review,” *European Polymer Journal*, vol. 79, pp. 36–62, 2016.

[23] T.-N. Zhou, Z.-C. Hou, K. Wang, Q. Zhang, and Q. Fu, “Polystyrene-wrapping multi-walled carbon nanotubes obtained via simple physical modification of melt mixing,” *Polymers for Advanced Technologies*, Sep. 2009.

[24] A. S. Patole, S. P. Patole, J.-B. Yoo, J.-H. An, and T.-H. Kim, “Fabrication of polystyrene/multiwalled carbon nanotube composite films synthesized byin situmicroemulsion polymerization,” *Polymer Engineering & Science*, vol. 53, no. 6, pp. 1327–1336, 2012.

[25] Q. Wang and H. Moriyam, “Carbon Nanotube-Based Thin Films: Synthesis and Properties,” *Carbon Nanotubes - Synthesis, Characterization, Applications*, 2011.

[26] M. Olek, J. Ostrander, S. Jurga, H. Möhwald, N. Kotov, K. Kempa, and M. Giersig, “Layer-by-Layer Assembled Composites from Multiwall Carbon Nanotubes with Different Morphologies,” *Nano Letters*, vol. 4, no. 10, pp. 1889–1895, 2004.

[27] D.-Y. Khang, J. A. Rogers, and H. H. Lee, “Mechanical Buckling: Mechanics, Metrology, and Stretchable Electronics,” *Advanced Functional Materials*, vol. 19, no. 10, pp. 1526–1536, 2009.

[28] G. M. Whitesides, N. Bowden, S. Brittain, A. G. Evans, and J. W. Hutchinson, “Nature,” *Nature*, vol. 393, no. 6681, pp. 146–149, 1998.

[29] C. M. Stafford, S. Guo, C. Harrison, and M. Y. M. Chiang, “Combinatorial and high-throughput measurements of the modulus of thin polymer films,” *Review of Scientific Instruments*, vol. 76, no. 6, p. 062207, 2005.

[30] D.-Y. Khang, J. Xiao, C. Kocabas, S. Maclaren, T. Banks, H. Jiang, Y. Y. Huang, and J. A. Rogers, “Molecular Scale Buckling Mechanics in Individual Aligned Single-Wall Carbon Nanotubes on Elastomeric Substrates,” *Nano Letters*, vol. 8, no. 1, pp. 124–130, 2008.

[31] E. K. Hobbie, T. Ihle, J. M. Harris, and M. R. Semler, “Empirical evaluation of attractive van der Waals potentials for type-purified single-walled carbon nanotubes,” *Physical Review B*, vol. 85, no. 24, 2012.

[32] M. R. Semler, J. M. Harris, A. B. Croll, and E. K. Hobbie, “Localization and length-scale doubling in disordered films on soft substrates,” *Physical Review E*, vol. 88, no. 3, 2013.

[33] M. R. Semler, J. M. Harris, and E. K. Hobbie, “Wrinkling and folding of nanotube-polymer bilayers,” *The Journal of Chemical Physics*, vol. 141, no. 4, p. 044901, 2014.

[34] E. Almutairi, M. Alzaid, A. M. N. Taufique, M. R. Semler, and E. K. Hobbie, “Rigidity of lamellar nanosheets,” *Soft Matter*, vol. 13, no. 13, pp. 2492–2498, 2017.

[35] C. M. Stafford, B. D. Vogt, C. Harrison, D. Julthongpiput, and R. Huang, “Elastic Moduli of Ultrathin Amorphous Polymer Films,” *Macromolecules*, vol. 39, no. 15, pp. 5095–5099, 2006.

[36] M. R. Semler, J. M. Harris, A. B. Croll, and E. K. Hobbie, “Localization and length-scale doubling in disordered films on soft substrates,” *Physical Review E*, vol. 88, no. 3, 2013.

[37] E. K. Hobbie, D. O. Simien, J. A. Fagan, J. Y. Huh, J. Y. Chung, S. D. Hudson, J. Obrzut, J. F. Douglas, and C. M. Stafford, “Wrinkling and Strain Softening in Single-Wall Carbon Nanotube Membranes,” *Physical Review Letters*, vol. 104, no. 12, 2010.

[38] J. M. Harris, J. Y. Huh, M. R. Semler, T. Ihle, C. M. Stafford, S. D. Hudson, J. A. Fagan, and E. K. Hobbie, “Elasticity and rigidity percolation in flexible carbon nanotube films on PDMS substrates,” *Soft Matter*, vol. 9, no. 48, p. 11568, 2013.

[39] J. M. Harris, G. R. S. Iyer, D. O. Simien, J. A. Fagan, J. Y. Huh, J. Y. Chung, S. D. Hudson, J. Obrzut, J. F. Douglas, C. M. Stafford, and E. K. Hobbie, “Structural Stability of Transparent Conducting Films Assembled from Length Purified Single-Wall Carbon Nanotubes,” *The Journal of Physical Chemistry C*, vol. 115, no. 10, pp. 3973–3981, 2011.

[40] E. Almutairi, M. Alzaid, A. M. N. Taufique, M. R. Semler, and E. K. Hobbie, “Rigidity of lamellar nanosheets,” *Soft Matter*, vol. 13, no. 13, pp. 2492–2498, 2017.

[41] J. M. Torres, C. M. Stafford, and B. D. Vogt, “Impact of molecular mass on the elastic modulus of thin polystyrene films,” *Polymer*, vol. 51, no. 18, pp. 4211–4217, 2010.

[42] E. K. Hobbie, D. O. Simien, J. A. Fagan, J. Y. Huh, J. Y. Chung, S. D. Hudson, J. Obrzut, J. F. Douglas, and C. M. Stafford, “Wrinkling and Strain Softening in Single-Wall Carbon Nanotube Membranes,” Physical Review Letters, vol. 104, no. 12, 2010.

[43] D. R. Askeland, P. P. Phule, and W. J. Wright, The Science and engineering of materials: sixth edition. Mason, OH: Cengage Learning, 2011.

[44] E. Almutairi, M. Alzaid, A. M. N. Taufique, M. R. Semler, and E. K. Hobbie, “Rigidity of lamellar nanosheets,” *Soft Matter*, vol. 13, no. 13, pp. 2492–2498, 2017.

APPENDIX. AFM MEASUREMENT

Atomic force microscopy (AFM) was used to obtain the thickness of SWCNT/PS films. A Veeco DI-3100 atomic force microscope was operated in tapping mode and an NT-MDT FMG01 probe with a tip radius of 10 nm was used. To obtain PS film thickness, for example, we first saved the topographic images that we obtained from AFM as shown in Figure A1.

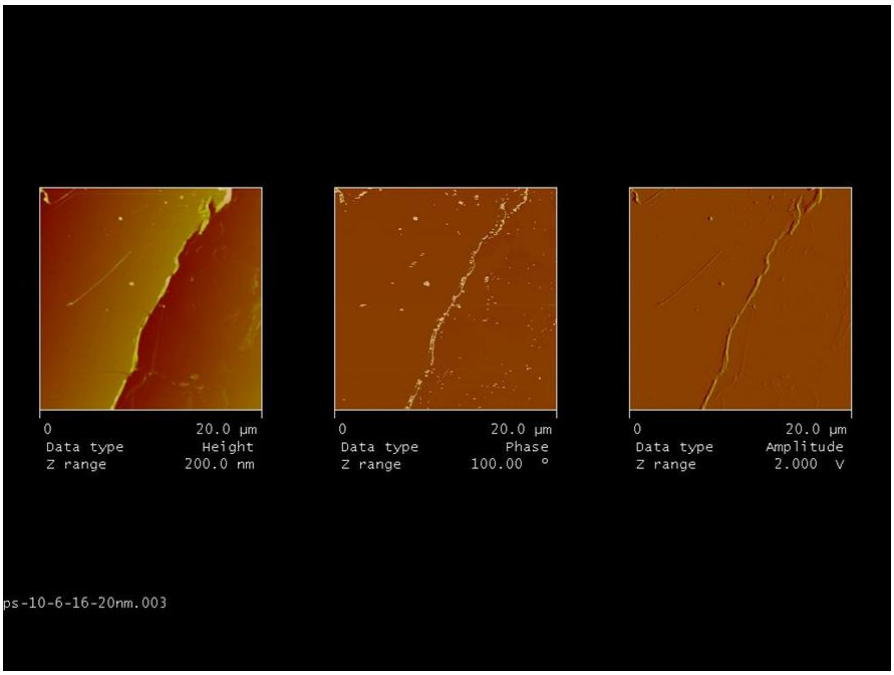

Figure A1. Topographic AFM images for a PS film of 10 nm targeted thickness.

We opened the images with ImageJ and converted the image to 32 bit. Then, we selected a rectangular area at the interface between the silicon surface and the PS film that was homogenous and free from dirt or defects. After that, we rotated the image so that the interface was parallel to the preview selection line, as shown in Figure A2.

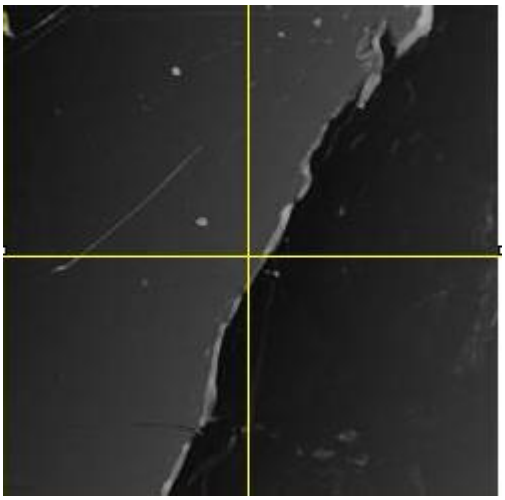

Figure A2. AFM image of a PS film of 10 nm targeted thickness before aligning the interface.

After aligning the interface with the grid, we made a plot profile of the image. By plotting the data as a graph, we subtracted the background of the substrate values to get the step size, where the resulting difference quantifies the thickness of the film. In this example, this gives us a precise value of h_0 = 11.2 nm for a film that was targeted to be 10 nm. The graph and the step-height profile are shown in Figure A3.

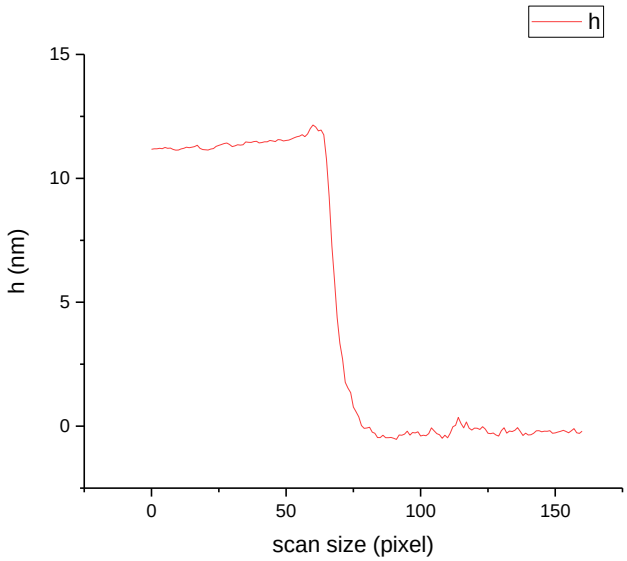

Figure A3. Step-height profile for a PS layer of 10 nm targeted thickness.